International Journal of Disaster Risk Reduction 36 (2019) 101088

Contents lists available at ScienceDirect

International Journal of Disaster Risk Reduction

journal homepage: www.elsevier.com/locate/ijdrr

Monitoring and forecasting of tropical cyclones: A new information-modeling tool to reduce the risk

Costas A. Varotsos[a,*], Vladimir F. Krapivin[b], Vladimir Yu. Soldatov[b]

[a] National and Kapodistrian University of Athens, Faculty of Physics, Department of Environmental Physics and Meteorology, University Campus Bldg. Phys. V, Athens, 15784, Greece

[b] Kotelnikov Institute of Radioengineering and Electronics, Russian Academy of Sciences, Moscow, Russia

ARTICLE INFO

Keywords:
Tropical cyclones disasters
Information theory
Franklin
Harvey
Irma and Katia tropical cyclones
Cyclone forecasting

ABSTRACT

Tropical cyclones are natural meteorological phenomena that are sometimes beneficial and sometimes dangerous. Beneficial because they can carry rain in the dry areas and transfer heat from the tropical regions to the higher latitudes. Dangerous because they can cause many disasters, such as heavy rain, strong winds, heavy shore storm waves and tornadoes. Of course, the extent of these disasters, which are very dangerous to people's life, depends largely on the intensity, size and location of this phenomenon. For these reasons, the development of reliable models for timely forecasting and monitoring of these phenomena is vital, especially as climate change is thought to increase both their frequency and intensity. This paper proposes an information-modeling tracker (IMT) of tropical cyclones based on the cluster algorithm to assess the instability of the atmosphere-ocean system. To this end, an instability indicator of the atmosphere-ocean system (IIAOS) is developed to form the basis for IMT synthesis and to be used as a precursor for the onset of tropical cyclones. Harmonization of IIAOS with the well-established Saffir-Simpson scale is carried out allowing the assessment of tropical cyclones characteristics, including their strength, and providing the basis for real-time atmosphere-ocean diagnostics. Finally, the IMT results obtained for a set of tropical cyclones (e.g., Franklin, Harvey, Irma and Katia) are presented and can be characterized as encouraging. Therefore, the functional IMT structure synthesized in this study can be used reliably as part of the global ocean monitoring system to reduce the risk from tropical cyclones.

1. Introduction

The tropical cyclones are intense tropical low pressure weather systems that occur more often in the northern than the southern hemisphere [1]. Their development is complex with three main structural features: the eye (the centre of the cyclone with the lowest atmospheric pressure on the surface), the eyewall (a region of cumulonimbus clouds around the eye) and the spiral rain bands.

The tropical cyclones (hurricanes and typhoons) are considered as the most dangerous and catastrophic natural disasters. Territories from more than 50 countries where about half of the world's population live are affected by tropical cyclones.

Most damages from hurricanes and typhoons are caused by strong winds, intense rainfall and floods. In general, three risk categories are assigned:

- Primary risk involving disastrous winds, debris and storm surge.
- Secondary risk covering fires and floods of fresh water.
- Tertiary risk involving losses of agricultural origin, poisoning of drinking water and human diseases.

These risks from tropical cyclones also cause annual losses in the economy of many countries. Therefore, detailed study and monitoring of these catastrophic phenomena is important for the deciding on the effective measures to be taken to alert the population in time to reduce the impacts both on the economy and on deaths.

The problem of tropical cyclogenesis is inseparably linked to global changes due to climate variability. Under this, particular attention is paid to investigations of the atmosphere-ocean system considering different space-time scales [2–4]. The complexity of the arising problems is determined by the instability of the atmosphere-ocean system. The tropical cyclones, their generation and their evolution have a stochastic character, and in this context, the detection and forecasting of these atmospheric processes require the development of non-traditional approaches. The most difficult task is the timely detection of a tropical cyclone manifestation, which is mainly based on exploring the state

* Corresponding author.
E-mail address: covar@phys.uoa.gr (C.A. Varotsos).

https://doi.org/10.1016/j.ijdrr.2019.101088
Received 24 October 2018; Received in revised form 30 January 2019; Accepted 8 February 2019
Available online 10 February 2019
2212-4209/ © 2019 Elsevier Ltd. All rights reserved.

Table 1
The characteristics of the atmosphere-ocean system to be used to estimate instability.

Characteristic	Identifier	Description of the characteristic
Ocean surface temperature, ˚C	x_1	Temperature is measured at depths of 1.0 m or 1.5 m depending on the buoy station type with a precision of ± 0.003 ˚C - ± 0.02 ˚C. The temperature satellite measurements correspond to depths of 10 μm to 1 mm depending on the use of infrared and microwave radiometers, respectively.
Wind speed, m/s	x_2	Wind speed is measured at buoy stations at an altitude of 3.5m with a precision of 3%. The wind speed at the surface of the ocean is also estimated on the basis of satellite measurements of the emissivity and backscattering properties of the liquid surface, which provides the basis for estimating winds from space-borne passive and/or active microwave sensors.
Wind direction	x_3	Wind direction is determined with a precision of 5.0˚–7.8˚.
Precipitation (mm/h)	x_4	Precipitation is recorded every 10 min at the altitude of 3.5 m with a precision of ± 0.4 mm/h.
Sea water density, kg/m^3	x_5	Water density is calculated as a function of its salinity, temperature and pressure
Depth of the isotherm 20 ˚C	x_6	Depth of isotherm is calculated on the basis of vertical temperature distribution by means of linear interpolation with a step 20 m in depth.
Water temperature of fixed depths $\{h_i\}$, ˚C	$x_7(h_i)$	Water temperature is measured up to 750 m on fixed horizons with a precision of ± 0.02 ˚C.
Relative humidity of atmospheric air, %	x_8	Air humidity is measured at the altitude of 2.2 m above sea level with a precision of ± 2.7%.
Atmospheric pressure, atm.	x_9	Atmospheric pressure is fixed with a precision of ± 0.01% at the altitude 3m above sea level.
Atmospheric temperature, ˚C	x_{10}	Atmospheric temperature is measured at the altitude of 2.2 m with a precision of ± 0.2 ˚C. Satellite temperature measurements are obtained from radiometric observations.
Sea water salinity, $^o/_{oo}$	x_{11}	Salinity is assessed from the data of water temperature and its conductivity with a precision of ± 0.02$^o/_{oo}$
Significant wave height, m	x_{12}	It is calculated as the average of the highest one-third of all wave heights over the 20-min sampling period. The ocean wave heights are estimated with a satellite altimeter radar.
Dominant wave period, s	x_{13}	Dominant or peak wave period is the period corresponding to the frequency band with the maximum value of spectral density (wave energy) in the non-directional wave spectrum. The dominant wave period represents the most energetic wave in the spectrum.
Average wave period, s	x_{14}	It is the period (seconds) of all waves during the 20-min period.
The direction from which the waves at the dominant period are coming, degrees	x_{15}	The units are degrees from true North, increasing clockwise, with North as 0 (zero) degrees and East as 90˚.
Dewpoint temperature, ˚C	x_{16}	Dewpoint temperature taken at the same height as the air temperature measurement.
Weather station visibility, nmi	x_{17}	Buoy stations are limited to report from 0 to 1.6 nmi.

parameters of an aquatory where atmospheric pressure is steadily decreasing over a set time. Such an approach takes place within the Hurricane Research Division of NOAA, where satellite and meteorological data are collected and processed to detect the necessary conditions for the formation of a tropical cyclone. Bell et al. [5] suggested that heat, moisture, and momentum exchange in the atmosphere-ocean interface are primary processes in the intensification and maintenance of tropical cyclones. However, these exchanges are related to atmosphere-ocean interactions when the tropical cyclone reaches a particular category on the Saffir-Simpson scale.

A special type of cyclones, the cutoff cyclones, were claimed to be significant mechanisms of stratosphere-troposphere-exchange mechanisms [6]. This exchange can be accomplished by convective or radiative erosion of the anomalously low tropopause. The latter is a particular feature of cutoff cyclones, and this exchange occurs by turbulent mixing near the jet stream associated with the cutoff system, or as a result of the tropopause folding along the flank of the system. However, it should be noted that the convective exchange induced by cutoff cyclones is generally small compared to the exchange caused by the tropopause folding associated with upper level cyclogenesis [7].

Most research on tropical cyclone genesis focus on investigation for correlations between atmosphere-ocean interactions and other environmental and geophysical processes, including solar activity and seismic processes. It was found that the most devastating tropical cyclones began when the water temperature was greater than 26.5 ˚C, especially when the Sun was active [8–10]. There is no doubt that the tropical cyclone system affects the heat transfer in the atmosphere-ocean interface due to the mixing of the upper ocean, which is intensified according to the maximum speed of the surface wind. Emanuel and Nolan [11] have promoted the hypothesis that tropical cyclones are the result of a subcritical bifurcation of normal atmospheric state, which allowed the development of a small parametric index calculated on the basis of absolute vorticity, relative humidity at 700 hPa, and magnitude of the wind shear vector from 850 hPa to 200 hPa. As shown by Varotsos and Efstathiou [12], tropical cyclogenesis is characterized by the long-term memory effect, suggesting a new view of the problem of the origin of tropical cyclones and their evolution. Indeed, the task of detecting tropical cyclogenesis is a traditional task of unknown signal extraction in a noised field.

This paper proposes a model of this signal as an indicator of instability of the atmosphere-ocean system (IIAOS) taking into account the data provided directly by the environmental monitoring systems. This may greatly contribute to reduce the risk of tropical cyclones since their monitoring and forecasting are part of the strategies that are widely used in this direction.

2. Methodology

2.1. Definition and application of instability indicator

Tropical cyclones are one of the many complex space-time chaotic processes of climate formation. Krapivin et al. [13] proposed a new approach to tackling the main objective of tropical cyclogenesis, which is to synthesize the indicator of the tropical cyclone precursor based on the data supplied by the TAO/TRITON/PIRATA/RAMA system. Indeed, the solution of this task relates to the assessment of the state of the atmosphere-ocean system and the detection of conditions when this system begins to change its phase state. In this context, Soldatov [14] applied cluster analysis to detect phase transitions in the evolution of the atmosphere-ocean system. In addition, Sukov et al. [15] used a sequential analysis to predict transient processes in the atmosphere-ocean system on the Saffir-Simpson scale.

These studies have shown that there is a universal indicator that reflects the behavior of the atmosphere-ocean system as a component of the global climate system, whose monitoring focuses on atmospheric circulation, tropical convection, and other oceanographic conditions. In other words, let the vector $x(x_1,\ldots,x_s)$ represents the state of the atmosphere-ocean system and formed by information sources, such as the buoy, land-based meteorological stations and satellites. The components of vector x are provided at discrete time moments $\{t_i\}$. The specification of the vector x components is shown in Table 1.

The vector x components reflect the degree of atmosphere-ocean variability through distance and time when some of their combinations correspond to high levels of turbulence. There are a number of different

indices that describe atmosphere-ocean interactions, including the origin of tropical cyclogenesis processes [16–18]. Each of these indices allows for the identification of the spatial and temporal position of certain atmospheric phenomena, such as the deeply convective process or the thunderstorm development. Grankov and Milshin [19] identified the correlation between the atmospheric moisture and thermal fluxes at the atmosphere-ocean boundary with radio-brightness temperatures as a precursor to the origin of the tropical cyclone. Krapivin et al. [13] analyzing the data from buoy weather stations and meteorological satellites have proposed a monitoring procedure based on the assessment of the instability of the atmosphere-ocean system. This procedure performs continuous observation of large oceanic aquatories by searching for and detecting changes in their environment [20–23]. Each of the vector x components plays a limited role in this procedure. Therefore, a generalized characteristic $\Xi(x,t,\varphi,\lambda)$ is introduced as an instability indicator of the atmosphere-ocean system. The function $\Xi(x,t,\varphi,\lambda)$ is the total change in the variable exchange rate of the vector x components averaged over a limited period of time. Finally, the function $\Xi(x,t,\varphi,\lambda)$ is defined by the following expression:

$$\Xi(x, t_i, \phi, \lambda) = \frac{1}{sm} \sum_{j=i}^{i+m} \sum_{k=1}^{s} \beta_k \alpha_k(x, t_j, \phi, \lambda) \tag{1}$$

where m is the length of the quasi-stationary period of observations to calculate average values of the ocean-atmosphere system characteristics; s is the number of registered parameters of IIAOS; β_k is the weighting coefficient for the k-th characteristic;

$$\alpha_k(x, t_j, \phi, \lambda) = \begin{cases} 1 \text{ when } \Delta x_k(t_j, \phi, \lambda) \cdot \Delta x_k(t_{j+1}, \phi, \lambda) \le 0, \\ 0 \text{ when } \Delta x_k(t_j, \phi, \lambda) \cdot \Delta x_k(t_{j+1}, \phi, \lambda) > 0 \end{cases}$$

where

$$\begin{aligned} \Delta x_k(t_j, \varphi, \lambda) &= x_k(t_j, \varphi, \lambda) - x_k(t_{j+1}, \varphi, \lambda);\ x_k(t_{j+1}, \varphi, \lambda) \\ &= x_k(t_j, \varphi, \lambda) - x_k(t_{j+2}, \varphi, \lambda) \end{aligned}$$

The last two expressions give the meaning of the instability indicator. In more detail, the formula $\Delta x_k(t_j,\varphi,\lambda) = x_k(t_j,\varphi,\lambda)\text{-}x_k(t_{j+1},\varphi,\lambda)$ provides the deviation of kth component value at the time t_j from its value at the next time t_{j+1}. In the same way, the formula $\Delta x_k(t_{j+1},\varphi,\lambda) = x_k(t_j,\varphi,\lambda)\text{-}x_k(t_{j+2},\varphi,\lambda)$ gives the deviation of kth component value at the time t_j from its value at the time t_{j+2} (i.e. over one step). If $\Delta x_k(t_j,\varphi,\lambda)$ and $\Delta x_k(t_{j+1},\varphi,\lambda)$ are both positive or negative, then we assume that the process is stable. If $\Delta x_k(t_j,\varphi,\lambda)$ and $\Delta x_k(t_{j+1},\varphi,\lambda)$ have opposite signs then we assume that an instability begins.

Based on the data of the environmental characteristics given in Table 1, the calculation of the instability indicator in spatial pixels in the studied area provides its statistics. This is analysed employing the sequential analysis algorithm, which allows for the calculation of the crossing probability of a certain threshold of the instability indicator. The Saffir-Simpson scale is considered as threshold. Therefore, the significance of the last two formulas consists in the one-step and two-step interchange for calculating the average. Parameters m and β_k are empirical coefficients. In this study $m = 7$ and $\beta_k = 1$.

These values were evaluated during series of simulation experiments. Certainly, weight coefficients β_k may have different significance depending on the environment state. However, this task is not considered here.

Fig. 1 demonstrates examples of the dynamics of the instability indicator calculated by formula (1) for the zones and times in which Harvey, Irma and Katia tropical cyclones operated. The raw data of the indicator are normalized by its maximum during the period considered. Of course, it is obvious that the coordination of IIAOS with the Saffir-Simson hurricane scale allows the identification and classification of tropical cyclone stages in real time based on the data provided by the network of weather stations, including buoy stations TAO/TRITON/PIRATA/RAMA, the Florida Automated Weather Network (FAWN), Regional Specialized Meteorological Centers (RSMC), National Data Buoy Centre (NDBC) stations and satellite observations. Certainly, the precision of these results depends on the data completeness and the components of the vector x that have been evaluated.

2.2. Detection of the tropical cyclone origin

The detection of the onset of a tropical cyclone in a given aquatory Ω refers to looking for a moment when the phase state of the atmosphere-ocean system changes significantly. As shown in Fig. 1, this change is described by the atmosphere-ocean instability indicator and its calculation over the entire area of the test region can help to detect such a moment.

Fig. 2 demonstrates an example of the IIAOS calculation in Miami (Florida) on September 11, 2017 when hurricane Irma was located in this area. The spatial distribution of IIAOS shows that, in practice, during September 11, the variations in the indicator will not exceed 25% for many buoy stations, with the exception of stations along the hurricane track, where its category changes from 1 to storm. Under this, Florida Peninsula is divided by two zones where IIAOS is significantly different. Thus, IIAOS spatial distribution control allows for identification of the atmosphere-ocean phase state and decision-making on possible cyclone tracking.

Fig. 3 illustrates the IMT functional structure and defines the procedure for searching and detecting the moment when the tropical cyclone starts. This scheme provides a regular control of the environmental elements in the given area where a tropical cyclone may appear.

The formation of the dynamic series $\{\Xi(x,t,\varphi,\lambda)\}$ and the statistical analysis provide a decision about its noise or signal character. In the later case, the final decision about the closest moment of a tropical cyclone incident is the prognosis procedure that begins when the cyclone type classification is performed by the Saffir-Simpson scale. Table 2 defines a relationship between the $\Xi(x,t,\varphi,\lambda)$ and Saffir-Simpson scales. This relationship was determined by the consideration of tropical cyclones that take place during different seasons and in various aquatories. The average tropical cyclone strength (TCS) can be calculated using the following equation:

$$TCS = \begin{cases} 5 + (9.68 - 2.65\Xi)\ln \Xi - 0.18(1 - \Xi)^{-0.23} \text{ when } \Xi \ge 0.6, \\ 1.073\Xi \text{ when } \Xi < 0.6. \end{cases} \tag{2}$$

Table 2 explains the relationship between the Saffir-Simpson index scales and the instability indicator. However, it should be clarified that the vertical spatial effects associated with wind speed and other environmental characteristics are not addressed in this paper. This problem requires a more complex examination, which is important and needs to be studied separately.

The multi-step search procedure of Fig. 3 and the data in Table 2 provide time detection when the random process $\{\nu = \Xi(x,t,\varphi,\lambda)\}$ intercepts the corresponding level y. As a result, the sequential procedure for calculating the probability of this event is used [15]:

$$P(\Xi \ge y) = W_c(y) = 1 - c^{1/2} y^{-3/2} \int_0^y z^{-3/2} \exp\{-0.5c(z + z^{-1} - 2)\} dz \tag{3}$$

where $c = (E\nu)^2/D(\nu)$.

Finally, the regular calculation of $\nu_i = \Xi(x,t_i,\varphi,\lambda)$ and the use of formula (3) allows the evaluation of the atmosphere-ocean phase change probability (AOPCP) as well as forecasting the tropical cyclone strength and its tracking. The calculation of integral (3) is complicated when $c \to \infty$ and $y \to 0$. In these cases, the following approximations apply [15]:

$$W_c(y) = = \varphi[(y - 1)c1/2 + O(1/c),$$

$$W_c(y) = \varphi[(y - 1)(c/y)^{1/2}] + \varphi[-(y + 1)(c/y)^{1/2}]\exp\{2c\},$$

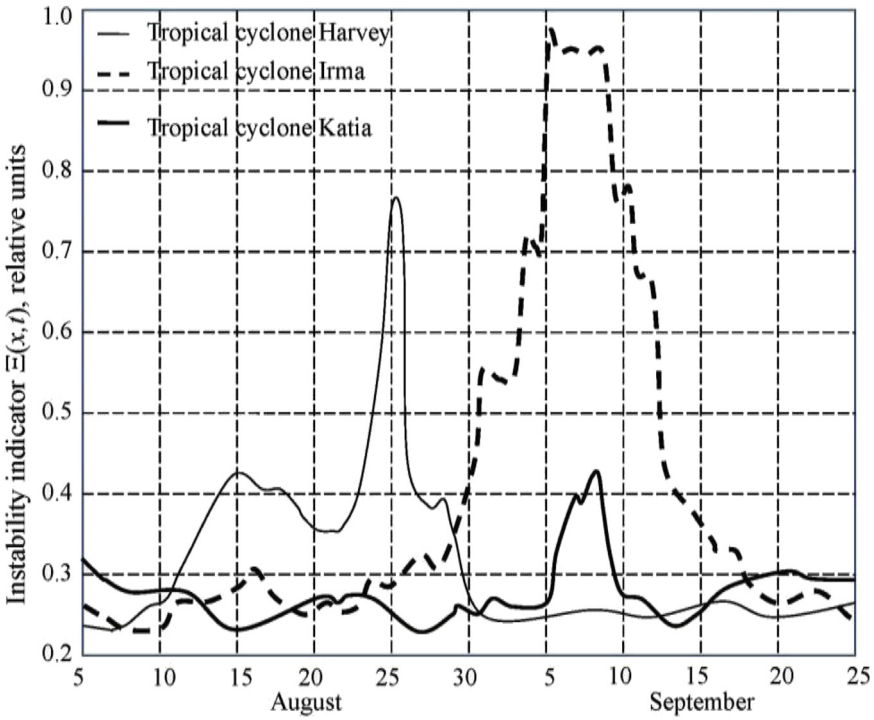

Fig. 1. The instability indicator dynamics in zones of Harvey, Irma and Katia tropical cyclones in the hurricane season of 2017. The atmosphere-ocean characteristics (see Table 1) were retrieved from the NDBC weather stations located in the Florida and Gulf of Mexico.

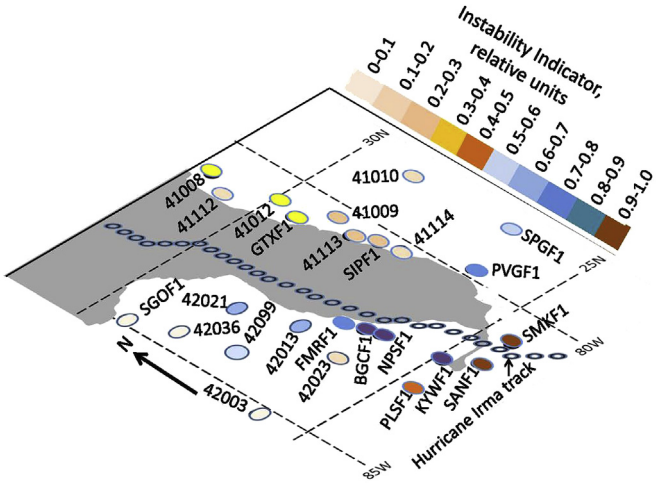

Fig. 2. The instability indicator calculated for September 11, 2017 using meteorological data from separate NDBC weather stations located in the Florida area.

where Φ is the normal distribution function.

3. Analysis and results

The statistical analysis of the series $\nu_{ij} = \Xi(x,t_i,\varphi_j,\lambda_j)$ allows for the detection of stable surges of the Instability Indicator Ξ in its dynamics in the considered aquatory that makes it possible to form a tropical cyclone track. The calculation of the probability of crossing the Ξ thresholds coordinated with the Saffir-Simpson scale provides the prognosis of a direction in which the tropical cyclone can move with high reliability.

Table 3 presents the IMT results obtained for several cases of tropical cyclones that examined in this study.

Fig. 4 shows successive steps when the IIAOS values are calculated within each pixel of the Floridian coastline.

Inspection of Fig. 4 shows that individual pixels sometimes reveal a signal that satisfies tropical depression or tropical storm, but this signal is chaotic in the aquatory which according to the rule of Fig. 3 cannot be a motive to decide on the beginning of these processes. Indeed, the increase in pixel density where the fixed IIAOS value exceeds the Saffir-Simpson scale corresponds to the hurricane's body. The eyewall structure that revealed in the Matthew hurricane is represented as a heterogeneous formation whose movement conforms to a real hurricane trajectory.

The simulation modeling results show that the optimal time interval to decide on the onset of tropical depression equals 5–7 h. After that, the signal is checked for possible movement in space. Fig. 3 defines a procedure that allows the signal to be tracked in its transformation by the transition between cyclone scales or its collapse. As can be seen from Fig. 5 the Tropical Pacific aquatory $(\varphi,\lambda)\in[13.4^{\circ}N, 46.7^{\circ}N]\cup[106.0^{\circ}E, 181.0^{\circ}E]$ is studied by the IIAOS stable features of the tropical cyclone after its formation and dissipation.

Fig. 6 gives an example of a tracking procedure for a Franklin tropical cyclone (2017). The position of the tropical cyclone is defined as a cluster of adjacent pixels in which the IIAOS value exceeds the background level and this complex moves into the aquatory. Therefore, this complex of pixels in its movement in space is characterized by the fixed IIAOS value boom that is considered as a detection signal, which is performed using the procedure of Fig. 3. In principle, this signal structure contributes to the estimation of the diameter of the hurricane eye and hurricane propagation zone with precision according to spatial resolution.

4. Conclusions and discussion

In this study, an information-modeling tracker was developed to create atmosphere-ocean instability maps in different aquatories based on meteorological stations and meteorological satellites data. The use of the instability indicator combined with the Saffir-Simpson scale helps in assessing the strength of the tropical cyclone with real time tracking.

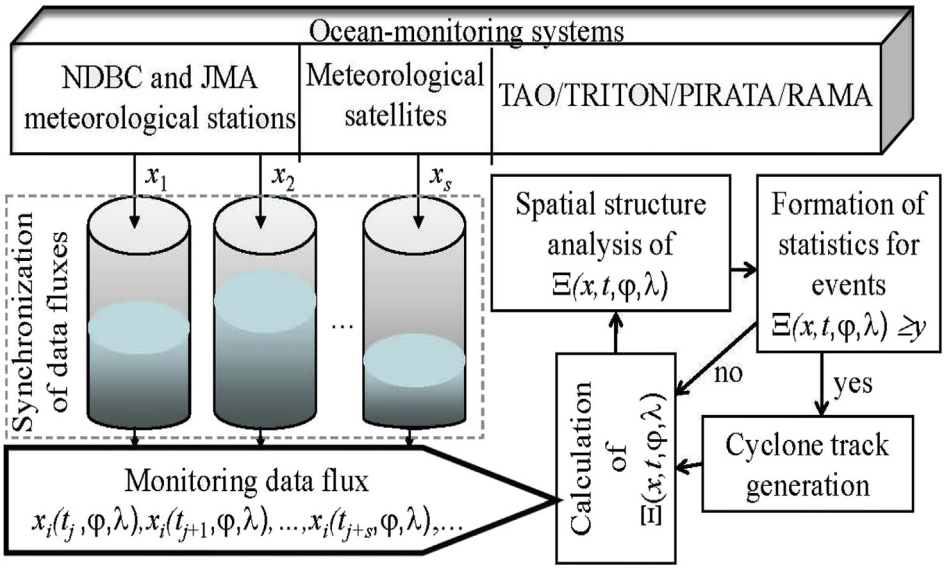

Fig. 3. The scheme of information-modeling tracking of tropical cyclones, including the search and tracing stages of the time when the phase state of the atmosphere-ocean system begins stable change with its amplitude being increased.

Table 2
The agreement between the $\Xi(x,t,\varphi,\lambda)$ and the Saffir-Simpson hurricane scales.

Sea-surface state. Saffir-Simpson scale.	$\nu = \Xi(x,t,\varphi,\lambda)$ scale	
	ν_{min}	ν_{max}
Background state	0	0.38 ± 0.02
Tropical depression	0.313 ± 0.017	0.475 ± 0.023
Tropical storm	0.475 ± 0.023	0.612 ± 0.019
Category 1	0.612 ± 0.019	0.713 ± 0.012
Category 2	0.713 ± 0.012	0.798 ± 0.016
Category 3	0.798 ± 0.016	0.885 ± 0.014
Category 4	0.885 ± 0.014	0.937 ± 0.013
Category 5	0.937 ± 0.013	1.0

Table 3
Characteristics of tropical cyclones calculated through the IMT for the cases examined in this study. It was considered that $\Delta\varphi = 0.2^\circ$ (22.12 km) and $\Delta\lambda = 0.2^\circ$ (21.92 km).

Tropical cyclone	Maximal eye diameter (km)	Maximal eyewall diameter (km)	Life cycle (h)	Path length (km)	Motion speed (km/h)		AOPCP	
					min	max	min	max
Harvey	23.9	239.2	292	5843	3.7	73.6	0.73	0.89
Irma	36.8	631.8	318	8491	16.5	36.8	0.87	0.91
Katia	18.4	128.8	92	480	3.7	12.9	0.82	0.92
Gert	16.3	201.7	114	4486	16.5	73.2	0.88	0.90
Franklin	22.1	167.2	91	2131	21.4	36.7	0.77	0.93
Banyan	0	184.1	174	4201	16.7	53.6	0.74	0.82
Hato	64.6	564.8	78	1234	9.9	21.7	0.79	0.88
Sanvu	36.8	331.2	126	4088	12.2	49.6	0.78	0.87
Doksuri	89.3	211.6	84	2104	16.5	37.8	0.81	0.90
Talim	91.7	467.2	238	3975	9.8	23.4	0.79	0.92
Pakhar	0	325.7	63	1922	25.1	33.6	0.76	0.89
Mawar	0	243.1	73	726	5.8	12.3	0.77	0.91
Guchol	0	199.5	54	1342	19.9	31.7	0.81	0.94
Matthew	45.9	279.3	269	5051	12.8	38.6	0.85	0.96

The monitoring scheme proposed here allows for the fixation and localization of geographical coordinates where the instability of the atmosphere-ocean system begins to rise steadily. According to Fig. 3, IMT can perform the following functions:

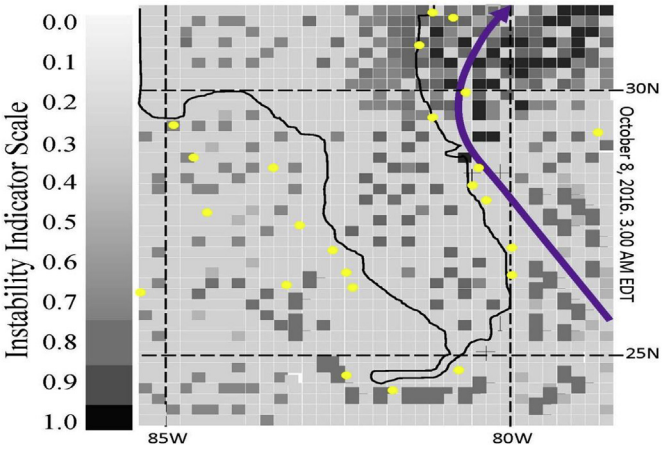

Fig. 4. The tropical cyclone tracking procedure realized for hurricane Matthew (October 2016). Weather stations are marked with a symbol •. The spatial resolution is 0.2° × 0.2°.

- Calculations of IIAOS in the pixels of oceanic aquatory based on meteorological data in real time.
- Stabilize pixels with consistent high IIAOS and form the dynamic series to make a statistical decision on the possible start of the tropical cyclone.
- Formation of spatial spots from neighboring pixels with high IIAOS and their dynamic control to form the eye and eyewall of the tropical cyclone.
- Tracking the tropical cyclone by estimating its intensity using the Saffir-Simpson scale.
- Assessing the response of the atmosphere-ocean system to the tropical cyclogenesis zone for climate changes under hypothetical scenarios.

The set of these functions distinguishes IMT from other existing similar systems such as the TEPS (Typhoon Ensemble Prediction System) developed at the Japan Meteorological Agency. The TEPS is oriented to a limited Pacific zone and uses a vector method for assessing a growth rate of the total energy perturbation [24]. There are many hurricane forecast models that solve the mathematical equations of the atmosphere dynamics and have a mainly theoretical sense [25].

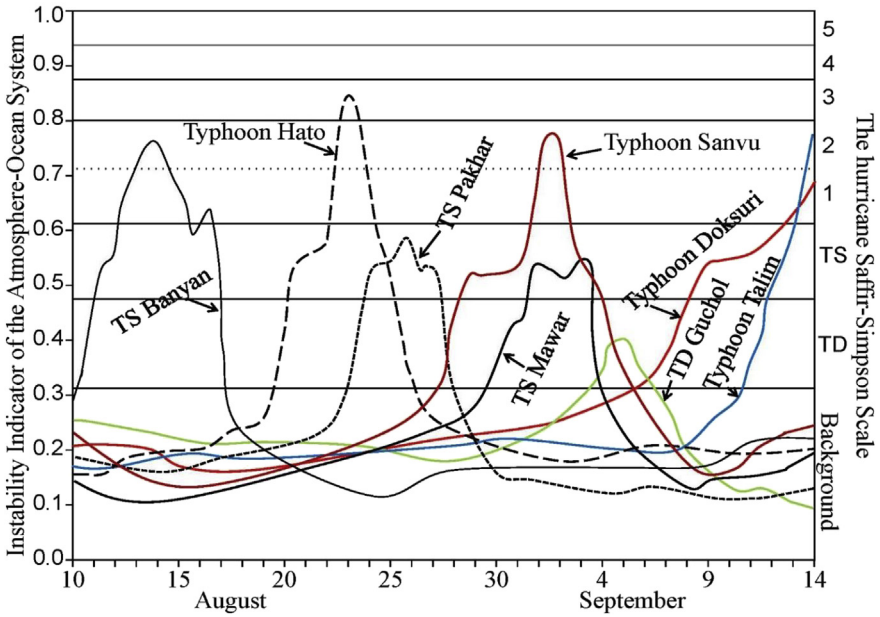

Fig. 5. Results of the Tropical Pacific aquatory diagnostics.

The simulation experiments performed here validate the efficiency of the IMT as a credible tool to solve the main tropical cyclogenesis task providing additional capabilities for existing ocean monitoring systems. Certainly, there are a number of unsolved tasks as topics for future studies. Particularly, the weighting coefficients β_k ($k = 1,\ldots, s$) require detailed analysis as a source of uncertainty. In this paper, $\beta_k = 1.0$ ($k = 1,\ldots, s$) which can be considered as a scenario. Preliminary assessments have shown that the role of the atmosphere-ocean characteristics changes with the evolution of tropical cyclones.

The process of increasing the IIAOS is accompanied by an increase in the role of wind parameters and the reduction of other features of the atmosphere-ocean system. Undoubtedly, there are unspecified tasks such as assessing the importance of data delivery systems for the vertical distribution of atmosphere-ocean characteristics (temperature, salinity, pressure, wind) [26–30]. However, the proposed model is a warning tool for the emergence of devastating tropical cyclones, and can be used to develop strategies and techniques to reduce the risk of cyclone disasters.

One might argue that the instability indicator proposed here has the potential to predict the genesis or development of a tropical cyclone. It might be considered that the instability indicator essentially reflects the current state of the atmosphere-ocean system in which a tropical cyclone may have already formed when IIAOS is high. Thus, to predict the tropical cyclone genesis at some location after several days, one has to use numerical models, which is definitely far more complex than the current system.

The answer to the above considerations is that the algorithm proposed here involves a regular calculation of the instability indicator in a controlled aquatory. As a result, the set of the instability indicator values at different coordinates are already available and therefore its

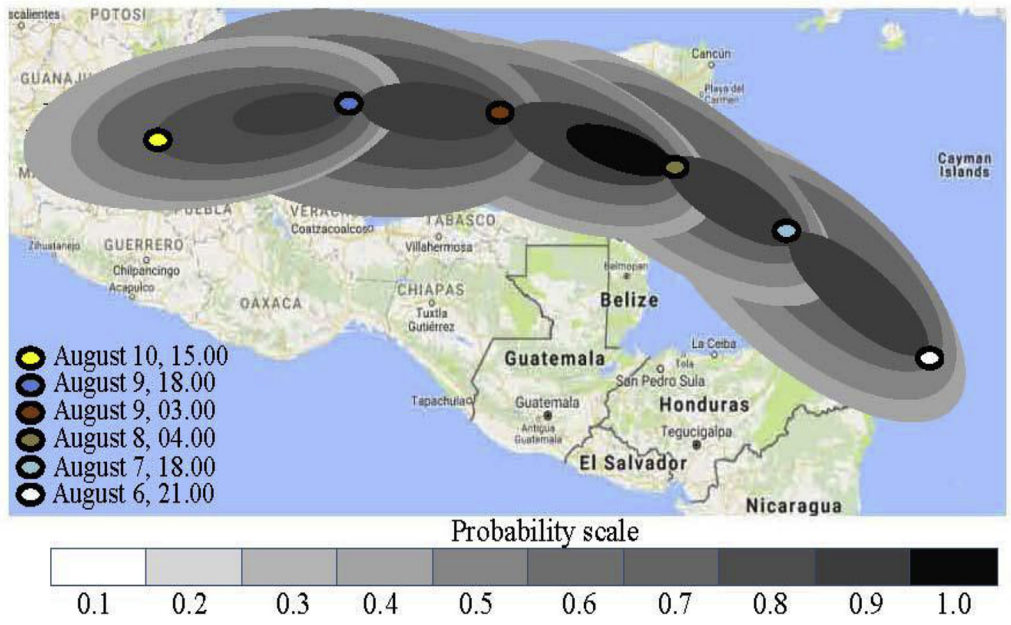

Fig. 6. Tracking of the Franklin tropical cyclone (2017) using IIAOS as part of the sequential search and prognosis procedure of Fig. 3.

future values can be predicted by using the sequential analysis method. Undoubtedly, the proposed method also allows monitoring of the aquatic environment. Of course, combining the use of the proposed method with cyclogenesis and climate models can provide a more efficient tool for forecasting tropical cyclones.

Another question that would most likely be asked is whether the proposed method in this study provides forecast or nowcast. From this point of view, one can argue that the proposed method only collects and illustrates observational data (or their linear combination) of the atmosphere-ocean system, which is more likely to be nowcast. Any forecast (predicting future state of the atmosphere-ocean system or the position of a tropical cyclone) should be based either on dynamical (e.g., fluid equations) or on statistical (e.g., lead-lag correlation) methods [31].

It is worth noting that nowcast refers to the use of data to assess the current dynamical state of a complex system. The goal of nowcast is to describe the present state of the system, distinct from the idea of forecast, which aims to describe the future state of the system [32–34]. Therefore, it could potentially be considered that the proposed method initially runs the forecast and subsequently the nowcast. Nowcast recently was based on the concept of "natural time" [35–38].

Finally, it would be very useful to describe the environment and cost for running the proposed tool, including platform, basic setup, updating frequency for display, how long the calculation takes once data transfer is completed etc. These details will help potential users who are interested in transplanting the proposed tool. This will be implemented in the follow-up paper when the information – instrumental tools for the synthesis of the monitoring system could be proposed and determine which satellites can be its components.

In conclusion, the proposed model is a warning tool for the emergence of devastating tropical cyclones, and can be used to develop strategies and techniques to reduce the risk of cyclone disasters. The vulnerability of the population to this risk has declined significantly over the last decades due to the continued implementation of combined strategies on this issue. Nevertheless, two very important issues still remain. First, the tropical cyclone warning, which causes indirect economic losses, is not determined solely by the wind speed. Secondly, enhanced protection helps citizens develop a strong sense of security against the risk of tropical cyclone. But this sense of security can be so strong that it incites a lack of sensitivity to the possible dangers of the tropical cyclone. Based on the above conclusions and in spite of the available forecasting tools, such as that proposed in this study, it is suggested that, in addition to the existing strategies for reducing tropical cyclone risk, additional strategies should be developed to reinforce the perception of risk of the community against risk [39].

References

[1] S.J. Camargo, A.G. Barnston, P.J. Klotzbach, C.W. Landsea, Seasonal tropical cyclone forecasts, World Meteorol. Organ. Bull. 56 (4) (2007) 297.

[2] M.N. Efstathiou, C.A. Varotsos, On the altitude dependence of the temperature scaling behaviour at the global troposphere, Int. J. Remote Sens. 31 (2) (2010) 343–349.

[3] C.A. Varotsos, M.N. Efstathiou, A.P. Cracknell, On the scaling effect in global surface air temperature anomalies, Atmos. Chem. Phys. 13 (10) (2013) 5243–5253.

[4] M.N. Efstathiou, C.A. Varotsos, Intrinsic properties of Sahel precipitation anomalies and rainfall, Theor. Appl. Climatol. 109 (3–4) (2012) 627–633.

[5] M.M. Bell, M.T. Montgomery, K.A. Emanuel, Air-sea enthalpy and momentum exchange at major hurricane wind speeds observed during CBLAST, American Meteorology Society, 2012, https://doi.org/10.1175/JAS-D-11-0276.1.

[6] C.A. Varotsos, K.Y. Kondratyev, Ozone dynamics over Greece as derived from satellite and in situ measurements, Int. J. Remote Sens. 16 (10) (1995) 1777–1798.

[7] J.R. Holton, P.H. Haynes, M.E. McIntyre, A.R. Douglass, R.B. Rood, L. Pfister, Stratosphere-troposphere exchange, Rev. Geophys. 33 (4) (1995) 403–439.

[8] K. Arora, P. Dash, Towards dependence of tropical cyclone intensity on sea surface temperature and its response in a warming world, Climate 4 (30) (2016), https://doi.org/10.3390/cli4020030.

[9] V.F. Krapivin, C.A. Varotsos, Modelling the CO2 atmosphere-ocean flux in the upwelling zones using radiative transfer tools, J. Atmos. Sol. Terr. Phys. 150 (2016) 47–54.

[10] J.B. Elsner, T.H. Jagger, R.E. Hodges, Daily tropical cyclone intensity response to solar ultraviolet radiation, Geophys. Res. Lett. 37 (2010) L09701, https://doi.org/10.1029/2010GL043091.

[11] K.A. Emanuel, D. Nolan, Tropical cyclone activity and the global climate system, Bull. Am. Meteorol. Soc. 85 (2004) 667–668.

[12] C.A. Varotsos, M.N. Efstathiou, Is there any long-term memory effect in the tropical cyclone? Theor. Appl. Climatol. 114 (2013) 643–650.

[13] V.F. Krapivin, V.Y. Soldatov, C.A. Varotsos, A.P. Cracknell, An adaptive information technology for the operative diagnostics of the tropical cyclones; solar terrestrial coupling mechanisms, J. Atmos. Sol. Terr. Phys. 89 (1) (2012) 83–89.

[14] V.Yu Soldatov, An information technology for the operative diagnostics of the ocean-atmosphere system, Proceedings of the International Symposium of Mathematical Modelling of Tropical Hurricane Beginning and Searching its Indicators-Precursors. 16 December 2009, Hochiminh City, Vietnam, Institute of Applied Mechanics and Informatics, Hochiminh City, 2009, pp. 65–85.

[15] A.I. Sukov, V.Yu Soldatov, V.F. Krapivin, A.P. Cracknell, C.A. Varotsos, A sequential analysis method for the prediction of tropical hurricanes, Int. J. Remote Sens. 29 (9) (2008) 2787–2798.

[16] P. Chang, S.G. Philander, A coupled ocean-atmosphere instability of relevance to the seasonal cycle, Am. Meteorol. Soc. 51 (24) (1994) 3627–3648 14.

[17] S. Queralt, E. Hernandez, D. Gallego, I. Iturrioz, Atmospheric instability analysis and its relationship to precipitation patterns over the western Iberian Peninsula, Adv. Geosci. 10 (2007) 39–44.

[18] V.P. Gorbatenko, S.Yu Krechetova, M.Yu Belikova, O.E. Nechepurenko, The comparison of atmospheric instability indices retrieved from the data of radio sounding and MODIS spectroradiometer on thunderstorm days over west siberia, Russ. Meteorol. Hydrol. 40 (5) (2015) 289–295.

[19] A.G. Grankov, A.A. Milshin, Microwave Radiation of the Ocean-Atmosphere: Boundary Heat and Dynamic Interaction, Springer, London, 2016, p. 314.

[20] K.Y. Kondratyev, V.F. Krapivin, Monitoring and prediction of natural disasters, Nuovo Cimento Soc. Ital. Fis., A C 27 (6) (2004) 657–672.

[21] K.Ya Kondratyev, V.F. Krapivin, C.A. Varotsos, Natural Disasters as Interactive Components of Global Ecodynamics, Springer/Praxis, Chichester, UK, 2006, p. 578.

[22] K.Y. Kondratyev, C. Varotsos, Atmospheric greenhouse effect in the context of global climate change, Il Nuovo Cimento C 18 (1995) 123–151.

[23] K.Y. Kondratyev, C.A. Varotsos, Volcanic eruptions and global ozone dynamics, Int. J. Remote Sens. 16 (1995) 1887–1895.

[24] M. Yamaguchi, R. Sakai, M. Kyoda, T. Komori, T. Kadowaki, Typhoon ensemble prediction system developed at the Japan Meteorological Agency, Mon. Weather Rev. 137 (2009) 2592–2604.

[25] V.G. Bondur, V.F. Krapivin, Space Monitoring of Tropical Cyclones, Scientific World, Moscow, 2009, p. 506 (in Russian).

[26] V.F. Krapivin, C.A. Varotsos, V.Yu Soldatov, New Ecoinformatics Tools in Environmental Science: Applications and Decision-Making, Springer, London, U.K., 2015, p. 903.

[27] M.N. Efstathiou, C.A. Varotsos, Intrinsic properties of Sahel precipitation anomalies and rainfall, Theor. Appl. Climatol. 109 (2012) 627–633.

[28] C.A. Varotsos, The global signature of the ENSO and SST-like fields, Theor. Appl. Climatol. 113 (2013) 197–204.

[29] C.A. Varotsos, C.L.E. Franzke, M.N. Efstathiou, A.G. Degermendzhi, Evidence for two abrupt warming events of SST in the last century, Theor. Appl. Climatol. 116 (2014) 51–60.

[30] Y. Xue, J. Ai, W. Wan, H. Guo, Y. Li, Y. Wang, J. Guang, L. Mei, H. Xu, Gridenabled high-performance quantitative aerosol retrieval from remotely sensed data, Comput. Geosci.-UK 37 (2011) 202–206.

[31] S. Lovejoy, C. Varotsos, Scaling regimes and linear/nonlinear responses of last millennium climate to volcanic and solar forcings, Earth Sys. Dyn. 7 (1) (2016) 133–150.

[32] J.R. Holliday, W.R. Graves, J.B. Rundle, D.L. Turcotte, Computing earthquake probabilities on global scales, Pure Appl. Geophys. 173 (3) (2016) 739–748.

[33] M. Luginbuhl, J.B. Rundle, D.L. Turcotte, Natural time and nowcasting earthquakes: are large global earthquakes temporally clustered? Earthquakes and Multi-Hazards Around the Pacific Rim, Vol. II 2019, Birkhäuser, Cham, 2018, pp. 137–146.

[34] C. Varotsos, The southern hemisphere ozone hole split in 2002, Environ. Sci. Pollut. Res. 9 (6) (2002) 375–376.

[35] N.V. Sarlis, E.S. Skordas, P.A. Varotsos, A. Ramiriez-Rojas, E.L. Flores-Marquez, Natural time analysis: on the deadly Mexico M8.2 earthquake on 7 September 2017, Physica A 506 (2018) 625–634.

[36] P.A. Varotsos, N.V. Sarlis, E.S. Skordas, Natural Time Analysis: The New View of Time, Springer, Berlin, 2011.

[37] P.A. Varotsos, N.V. Sarlis, H.K. Tanaka, E.S. Skordas, Some properties of the entropy in natural time, Phys. Rev. E 71 (2005) 032102.

[38] N.V. Sarlis, E.S. Skordas, P.A. Varotsos, T. Nagao, M. Kamogawa, H. Tanaka, S. Uyeda, Minimum of the order parameter fluctuations of seismicity before major earthquakes in Japan, Proc. Nat. Acad. Sci. 110 (34) (2013) 13734–13738.

[39] L. Fok, L.T. Cheung, Evaluating the impact reduction strategies for the tropical cyclone hazard in Hong Kong, Asian Geogr. 29 (2) (2012) 121–129.